Quantifying losses and thermodynamic limits in nanophotonic solar cells

Sander A. Mann,[1*] Sebastian Z. Oener,[1*] Alessandro Cavalli,[2] Jos E. M. Haverkort,[2] Erik P.A.M. Bakkers,[2,3] and Erik C. Garnett[1,†]

[1]Center for Nanophotonics, FOM Institute AMOLF, Science Park 104, 1098 XG Amsterdam, The Netherlands
[2]Applied Physics, Eindhoven University of Technology, PO Box 513, 5600 MB Eindhoven, The Netherlands
[3]Kavli Institute of Nanoscience, Delft University of Technology, The Netherlands
**These authors contributed equally to the work.*
†To whom correspondence should be addressed. E-mail: garnett@amolf.nl

Nanophotonic engineering holds great promise for photovoltaics: the record conversion efficiencies of nanowire solar cells are increasing rapidly[1,2], and the record open-circuit voltages are becoming comparable to record planar equivalents[3,4]. Furthermore, several authors have suggested that nanophotonic effects such as large absorption cross sections can reduce cost and increase efficiencies with respect to planar solar cells[5,6]. These effects are particularly pronounced in single nanowire devices, where two out of the three dimensions are subwavelength. Therefore, single nanowire devices provide an ideal platform to study how nanophotonics affects photovoltaics[7–12]. However, for these devices the standard definition of power conversion efficiency no longer applies, because the nanowire can absorb light from an area much larger than its own size[6]. Additionally, the thermodynamic limit on the photovoltage is a priori unknown and may be very different from that of a planar solar cell. This complicates characterization and optimization of such nanoscale devices. Here we analyse an InP single nanowire solar cell using intrinsic metrics to place its performance on an absolute thermodynamic scale

and pinpoint performance loss mechanisms. Determining these metrics requires integrating sphere microscopy, which enables simultaneous and spatially resolved quantitative absorption, internal quantum efficiency (IQE), and photoluminescence quantum yield (PLQY) measurements. For our record device we measure a photocurrent collection efficiency of >90% and an open-circuit voltage (850 mV) that is 73% of the thermodynamic limit (1.16 V).

The single nanowire device consists of a 310 nm diameter wurtzite InP nanowire with a 50 nm SiO_2 coating used to prevent oxidation and enhance stability (see Fig. 1a and Methods). It has a short-circuit current of I_{sc} = 450 pA, an open-circuit voltage of V_{oc}= 850 mV, and a fill factor of FF = 0.76 under AM1.5 solar spectrum illumination (Fig. 1b), all of which are high compared to previous nanowire devices. However, to understand the origin of the obtained I_{sc} and V_{oc} we need to determine intrinsic metrics like the device IQE and PLQY. To date the primary experimental challenge in determining these performance metrics for single nanowire devices has been measuring quantitative absorption during solar cell operation, which is not possible with existing techniques[13]. These methods assume that absorbed power is converted into heat (photothermal spectroscopy[14,15]), that the nanoparticle does not scatter (spatial modulation extinction spectroscopy[16,17]), or that the particle is an ideal dipole (scattered field interferometry[18]). Integrating sphere microscopy circumvents these assumptions by combining the standard tool for measuring absorptance of macroscopic samples[19] or ensembles of nanoparticles[20], with a long working distance microscope objective (see Fig. 1c). This technique measures all power that is not absorbed (reflected,

transmitted, and scattered), allowing the absorbed power to be determined directly from a simple energy balance (see Fig. 1 and Methods for further details).

Two-dimensional maps of the absorptance (fraction of incident power that is absorbed) and IQE (fraction of absorbed light converted to current) are shown in Fig. 2. A top view SEM image of the device is shown in Fig. 2a for comparison to the absorptance and IQE maps in Fig. 2b and 2c, measured at an excitation wavelength of 600 nm. The IQE reaches a peak value of 100% and is strongly localised to the upper half of the wire, as is more clearly visible in the line profile of the IQE along the nanowire in Fig. 2d. The colour shading in Fig. 2d shows the intended doping profile during nanowire growth. Carrier collection is most efficient near the n-type/intrinsic interface, and collection occurs over a length of 3.4 microns. In the p-type region the IQE is essentially zero, indicating short electron diffusion lengths. This is confirmed by an electron-beam induced current (EBIC) measurement shown above the IQE line profile, from which we determine the electron diffusion length in the intrinsic/p-type segment to be 285 nm (see Figure S1). The IQE is nearly independent of polarisation and wavelength, with values >90% over the whole wavelength range up to the band gap (Fig. 2e). The small difference in band gap depending on excitation polarisation is caused by the anisotropic nature of wurtzite InP and has previously been observed with photoluminescence excitation spectroscopy[21].

With integrating sphere microscopy we can probe not only the IQE to understand the current collection efficiency, but also directly measure the PLQY[20,22]. In absence of non-radiative recombination, PLQY=1 and the open-circuit voltage

reaches the thermodynamic limit V_{oc}^{rad}. For a PLQY below 1, the V_{oc} is reduced from the radiative limit to the implied $V_{oc}^{imp} = V_{oc}^{rad} - V_T|ln\,(PLQY)|$, where V_T is the thermal voltage (25.9 mV)[23,24]. Hence, the PLQY plays a crucial role in understanding the photovoltage. To measure the PLQY, we place a filter in front of the integrating sphere photodetector, such that only photoluminescence is detected (see Methods). Our spatially-resolved measurements show that the nanowire PLQY peaks in the same region where the IQE is highest (Fig. 3a), with an average PLQY over the active area of 0.9% at an excitation intensity of 1 μW 600 nm light (~1.4×10^3 suns, note that the PLQY is independent of excitation wavelength as shown in Fig. S2). To determine the average PLQY at 1 sun intensity, we measure at a range of lower excitation powers (Fig. 3b). The PLQY decreases linearly with excitation intensity, indicating that in this regime Shockley-Read-Hall recombination dominates (see Supplementary Section 3). Assuming linearity down to 1 sun intensity, the average PLQY is 4.0×10^{-4} (0.040%). This value corresponds to a V_{oc} loss of 210 mV from the thermodynamic limit, and is comparable to what is observed in world record planar crystalline Si, Cu(In,Ga)Se_2, and InP solar cells[24].

The PLQY can provide the V_{oc} loss from the thermodynamic bound V_{oc}^{rad}, but in order to calculate the latter value for our device we must know the recombination current corresponding to radiative thermal emission, I_0^{rad}. This emission current together with the I_{sc} determines $V_{oc}^{rad} = V_T\,ln\left(I_{sc}/I_0^{rad}\right)$[23]. In a macroscopic solar cell, the I_{sc} and I_0^{rad} can be calculated by integrating the external quantum efficiency (EQE, fraction of incident photons converted to current) over the solar and blackbody spectra (T=300K), respectively[24]. However, for single nanowire solar

cells the standard definition of EQE is not valid, because the absorption cross section (σ_{abs}) can be much larger than the device area. To solve this important issue, we define a new quantity called the collection cross section that takes on the same role:

$$\sigma_{EQE}(\lambda, \Omega) = \int IQE(\lambda, z)\, \sigma_{abs}^{1D}(\lambda, \Omega)\, dz \qquad \text{(Eq. 1)}$$

where $IQE(\lambda, z)$ is the spatially resolved internal quantum efficiency (shown in Fig. 2e) and $\sigma_{abs}^{1D}(\lambda, \Omega)$ is the effective absorption width of the nanowire (determined from the absorptance, see Methods and Supplementary Section 4). Fig. 4a shows σ_{EQE} for the nanowire device studied here, in both polarisations. Note that σ_{EQE} requires units of area, while the conventional EQE is a unitless quantum efficiency. This is a crucial difference, because for macroscopic solar cells the area collecting photons is independent of the incident wavelength and simply equal to the geometric area. In contrast, for nanostructures the interaction area with the incident light can be strongly wavelength dependent,[6] e.g. due to resonances[25]. Additionally, in contrast to the IQE and PLQY, σ_{EQE} can be determined directly from the photocurrent measurement, incident flux, and laser spot size, and an integrating sphere is thus not required (see Methods).

Integrating σ_{EQE} over the black body spectrum and all angles we find $I_0^{rad} = 3.1{\times}10^{-17}\ pA$, which leads to a maximum open-circuit voltage $V_{oc}^{rad} = 1.16\ V$ for our nanowire device (see Supplementary Section 5). The difference between the ideal voltage (V_{oc}^{rad}) and the measured V_{oc} (850 mV) is 310 mV: the V_{oc} is 73% of the thermodynamic limit. The measured V_{oc} is 100 mV smaller than the implied open-

circuit voltage V_{oc}^{imp} in the semiconductor nanowire, suggesting that the contact selectivity plays a significant role in the V_{oc} loss, likely due to diffusion of the highly mobile Zn out of the p-type doped region[26] and/or Fermi level pinning due to the surface oxide[27]. Additionally, knowledge of I_{sc} and I_0^{rad} allows us to determine the ideal fill factor, which is 89.5%, compared to 76% in our InP nanowire device. The deficit is likely due to large series resistance, which can also be observed from the slope of the I-V curve in Fig. 1b and is supported by a fit of the I-V curve (see Supplementary Section 6). The series resistance can most likely be reduced by increasing the contact quality and reducing the length of the intrinsic nanowire segment.

The V_{oc}^{rad} for this device is higher than the Shockley-Queisser V_{oc} for a planar cell with an absorption onset at 890 nm (see Fig. 4a), which is 1.13 V[28]. The difference arises due to suppressed absorption near the band gap, which thus leads to reduced emission and a lower radiative recombination current[29]. It is important to note that such a voltage enhancement due to suppressed absorption necessarily comes at a cost in current, and can therefore not lead to efficiencies above the Shockley-Queisser limit in macroscopic devices[30].

Integrating the EQE over the AM1.5 solar spectrum is a common procedure used in macroscopic solar cells to verify the I_{sc} from solar simulator measurements. Here we find that an analogous procedure using σ_{EQE} instead of EQE gives a calculated short-circuit current of 320 pA, which is 29% lower than the value measured under the solar simulator (450 pA). We attribute the difference to light trapping in the glass substrate, which leads to an overestimation of the actual

photocurrent. This is supported by the fact that covering almost the entire sample with opaque foil, including the nanowire, still results in a short-circuit current of ~100 pA (22% of total, see Supplementary Section 7). This suggests that just as with macroscopic solar cells, I_{sc} measurements under the solar simulator require proper masking to avoid artifacts. We therefore used the I_{sc} value based on σ_{EQE} for the calculation of V_{oc}^{rad} (see Supplementary Section 5).

In conclusion, integrating sphere microscopy measurements and analysis allow us to place nanoscale solar cell performance on an absolute thermodynamic scale and pinpoint loss mechanisms. These measurements may direct our efforts to make more efficient integrated power sources for autonomous nanoelectronic applications[7] or macroscopic nanowire solar cells that can beat record planar cell efficiencies. In terms of photocarrier collection, these nanowires are already close to the limit, reaching IQE values >90% in both polarisations for a 3.4 micron segment of the nanowire. In a vertical nanowire geometry, with the n-type segment facing the sun, this is enough to absorb all incident light and collect the generated carriers. Regarding the photovoltage, we determined three different values for the V_{oc} that can help us pinpoint remaining loss mechanisms (Fig. 4b): (1) the thermodynamic limit calculated from wavelength-dependent σ_{EQE} measurements (1.16 V), which only includes radiative recombination; (2) the material limit extracted from local PLQY measurements (950 mV), that includes non-radiative recombination in the nanowire; and (3) the device limit extracted from solar cell operation (850 mV), that also includes losses at the contacts. The 210 mV (18%) loss related to non-radiative recombination in the nanowire could be reduced by lowering the surface

recombination velocity (surface passivation) or material defect density (purification). Improvements in contact selectivity alone could lead to a 100 mV (12%) increase in the V_{oc} compared to our record single nanowire results. Combining both makes V_{oc} >1V for InP nanowire solar cells – far above world record planar InP solar cell performance – certainly within reach.

References

1. Aberg, I. *et al.* A GaAs Nanowire Array Solar Cell With 15.3% Efficiency at 1 Sun. *IEEE J. Photovoltaics* **6,** 185–190 (2016).
2. Wallentin, J. *et al.* InP Nanowire Array Solar Cells Achieving 13.8% Efficiency by Exceeding the Ray Optics Limit. *Science.* **339,** 1057–1060 (2013).
3. Kayes, B. M. *et al.* 27.6% Conversion efficiency, a new record for single-junction solar cells under 1 sun illumination. *Proceedings of the 37th IEEE Photovoltaic Specialists Conference*, 4–8 (2011)
4. Wanlass, M. Systems and methods for advanced ultra-high-performance InP solar cells. (2015).
5. Polman, A. & Atwater, H. A. Photonic design principles for ultrahigh-efficiency photovoltaics. *Nature Mater.* **11,** 174–177 (2012).
6. Krogstrup, P. *et al.* Single-nanowire solar cells beyond the Shockley–Queisser limit. *Nature Photon.* **7,** 306–310 (2013).
7. Tian, B. *et al.* Coaxial silicon nanowires as solar cells and nanoelectronic power sources. *Nature* **449,** 885–889 (2007).
8. Tang, J., Huo, Z., Brittman, S., Gao, H. & Yang, P. Solution-processed core–shell nanowires for efficient photovoltaic cells. *Nature Nanotech.* **6,** 568–572 (2011).
9. Holm, J. V *et al.* Surface-passivated GaAsP single-nanowire solar cells exceeding 10% efficiency grown on silicon. *Nat. Commun.* **4,** 1498 (2013).
10. Allen, J. E. *et al.* High-resolution detection of Au catalyst atoms in Si nanowires. *Nature Nanotech.* **3,** 168–173 (2008).
11. Nowzari, A. *et al.* A comparative study of absorption in vertically and laterally oriented InP core-shell nanowire photovoltaic devices. *Nano Lett.* **15,** 1809–1814 (2015).
12. Kelzenberg, M. D. *et al.* Photovoltaic Measurements in Single-Nanowire Silicon Solar Cells. *Nano Lett.* **8,** 710–714 (2008).
13. Crut, A., Maioli, P., Del Fatti, N. & Vallée, F. Optical absorption and scattering spectroscopies of single nano-objects. *Chem. Soc. Rev.* **43,** 3921 (2014).
14. Yorulmaz, M. *et al.* Single-Particle Absorption Spectroscopy by Photothermal Contrast. *Nano Lett.* **15,** 3041–3047 (2015).
15. Gaiduk, A., Yorulmaz, M., Ruijgrok, P. V & Orrit, M. Room-Temperature

Detection of a Single Molecule's Absorption by Photothermal Contrast. *Science.* **330,** 353–356 (2010).
16. Arbouet, A. *et al.* Direct Measurement of the Single-Metal-Cluster Optical Absorption. *Phys. Rev. Lett.* **93,** 127401 (2004).
17. Blancon, J.-C. *et al.* Direct measurement of the absolute absorption spectrum of individual semiconducting single-wall carbon nanotubes. *Nat. Commun.* **4,** 2542 (2013).
18. Husnik, M. *et al.* Quantitative Experimental Determination of Scattering and Absorption Cross-Section Spectra of Individual Optical Metallic Nanoantennas. *Phys. Rev. Lett.* **109,** 233902 (2012).
19. Burkhard, G. F., Hoke, E. T. & McGehee, M. D. Accounting for Interference, Scattering, and Electrode Absorption to Make Accurate Internal Quantum Efficiency Measurements in Organic and Other Thin Solar Cells. *Adv. Mater.* **22,** 3293–3297 (2010).
20. Gargas, D. J., Gao, H., Wang, H. & Yang, P. High Quantum Efficiency of Band-Edge Emission from ZnO Nanowires. *Nano Lett.* **11,** 3792–3796 (2011).
21. De Luca, M. *et al.* Polarized Light Absorption in Wurtzite InP Nanowire Ensembles. *Nano Lett.* **15,** 998–1005 (2015).
22. Leyre, S. *et al.* Absolute determination of photoluminescence quantum efficiency using an integrating sphere setup. *Rev. Sci. Instrum.* **85,** 123115 (2014).
23. Rau, U. Reciprocity relation between photovoltaic quantum efficiency and electroluminescent emission of solar cells. *Phys. Rev. B* **76,** 085303 (2007).
24. Green, M. A. Radiative efficiency of state-of-the-art photovoltaic cells. *Prog. Photovoltaics* **20,** 472–476 (2012).
25. Cao, L. *et al.* Engineering light absorption in semiconductor nanowire devices. *Nat. Mater.* **8,** 643–647 (2009).
26. Chu, S. N. G., Logan, R. A., Geva, M. & Ha, N. T. Concentration dependent Zn diffusion in InP during metalorganic vapor phase epitaxy. *J. Appl. Phys.* **78,** 3001 (1995).
27. Van Weert, M. H. M. *et al.* Large redshift in photoluminescence of p -doped InP nanowires induced by Fermi-level pinning. *Appl. Phys. Lett.* **88,** 043109 (2006).
28. Shockley, W. & Queisser, H. J. Detailed Balance Limit of Efficiency of p-n Junction Solar Cells. *J. Appl. Phys.* **32,** 510 (1961).
29. Sandhu, S., Yu, Z. & Fan, S. Detailed Balance Analysis and Enhancement of Open-Circuit Voltage in Single-Nanowire Solar Cells. *Nano Lett.* **14,** 1011–1015 (2014).
30. Yu, Z., Sandhu, S. & Fan, S. Efficiency above the Shockley–Queisser Limit by Using Nanophotonic Effects To Create Multiple Effective Bandgaps With a Single Semiconductor. *Nano Lett.* **14,** 66–70 (2014).

Acknowledgements

We acknowledge Albert Polman for use of lab space and equipment and for a thorough reading of the manuscript, Marco Seynen, Henk-Jan Boluijt, and Duncan Verheijde for technical support, and Henk-Jan Boluijt for the schematic diagram in Fig. 1c. We would like to thank Rene Van Veldhoven for the exceptional care of the MOCVD system, and Marcel Verheijen for the TEM measurements. We acknowledge Solliance for funding the TEM facility and the technical support from the NanoLab@TU/e cleanroom. The research leading to these results has received funding from the European Research Council under the European Union's Seventh Framework Programme ((FP/2007-2013)/ERC Grant Agreement No. 337328, "NanoEnabledPV"), the Dutch Technology Foundation STW (project 11826), which is part of the Netherlands Organization for Scientific Research (NWO), and the Dutch Ministry of Economic Affairs. This work is part of the research program of the Foundation for Fundamental Research on Matter (FOM), which is part of The Netherlands Organization for Scientific Research (NWO).

Author contributions

E.C.G., S.A.M., and S.Z.O. conceived the experiment, A.C., J.E.M.H., and E.P.A.M.B. synthesised the nanowires, S.Z.O. developed the contacting procedure, performed solar simulator and EBIC characterization, and S.A.M. developed integrating sphere microscopy and performed the optical measurements. All authors contributed to the manuscript.

Supplementary Information

Supplementary Information is available in the online version of the paper. Reprints and permission information is available online at www.nature.com/reprints. Correspondence and requests for materials should be addressed to E.C.G.

Competing financial interest

The authors declare no competing financial interests.

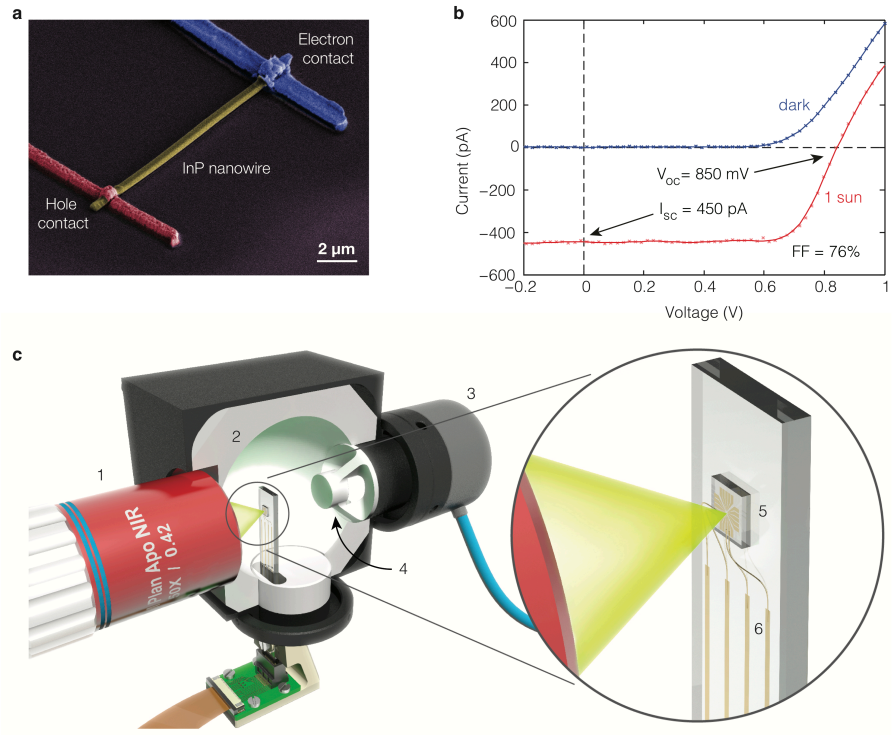

Figure 1 | Characterization of a record single nanowire solar cell. A single nanowire solar cell is characterized with integrating sphere microscopy. **a**. False-colour SEM image of the InP nanowire device (yellow) with hole contact (red) and electron contact (blue). **b**. The nanowire I-V curve in the dark (blue) and under the solar simulator at 1 sun intensity (red). The solid line is a smoothed fit to the data points (shown as small crosses). **c**. A schematic depicting the integrating sphere microscopy set-up. A microscope objective (1) focuses light from a monochromated supercontinuum laser source on the nanowire solar cell inside the integrating sphere. The integrating sphere (2, only half is shown) collects transmitted as well as scattered light via a photodetector (3) behind a baffle (4), while the objective directs the reflected light to another photodetector (not shown, see Fig. S3). Subtracting these calibrated signals from the input gives the local absorptance (fraction of incident light that is absorbed) with diffraction limited resolution. The device is connected to electrode pads (5) and current leads (6) to simultaneously measure photocurrent, enabling determination of the (IQE). With a long-pass filter in front of the detector (3), photoluminescence can be collected quantitatively to give the photoluminescence quantum yield (PLQY). The sample is mounted on a piezoelectric stage, enabling spatial mapping of all these output parameters.

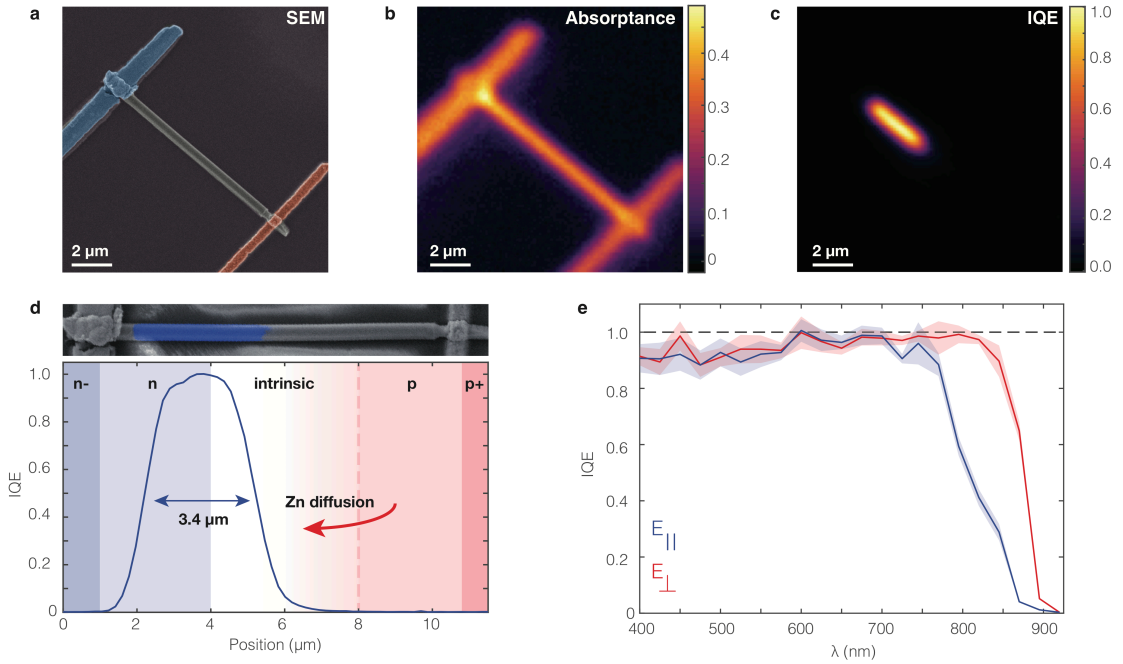

Figure 2 | Internal quantum efficiency of a single nanowire photovoltaic. By measuring quantitative absorption and photocurrent simultaneously the IQE can be determined with high spatial resolution. **a**. False colour scanning electron microscopy (SEM) image of the single nanowire device (InP nanowire diameter = 310 nm, length = 12.1 µm, SiO_2 shell thickness = 50 nm). The p-i-n doped InP nanowire device is visible in the center with an electron contact (blue) and hole contact (red). **b.** and **c**. Absorptance and internal quantum efficiency (IQE) as a function of position for the nanowire device. In **a-c** the scale bar is 2 µm. **d**. The IQE as a function of position along the nanowire length, convoluted with the focused spot size (beam radius 730 nm). The colour shading shows the nanowire doping profile as intended during nanowire growth. It should be noted that the p-type dopant zinc might have diffused further into the nanowire during growth, as it is very mobile in InP at high concentrations[26]. The SEM image on top has a superimposed electron beam-induced current (EBIC) measurement (blue shade) in good agreement with the IQE profile. **e**. The peak IQE spectrum for light polarised perpendicular (red) and parallel (blue) to the nanowire axis lies between 90% and 100% up to wavelengths close to the band gap, where the anisotropic nature of wurtzite InP becomes apparent**.** The shading displays the measurement uncertainty, which arises largely due to noise in the photodetectors (see Methods).

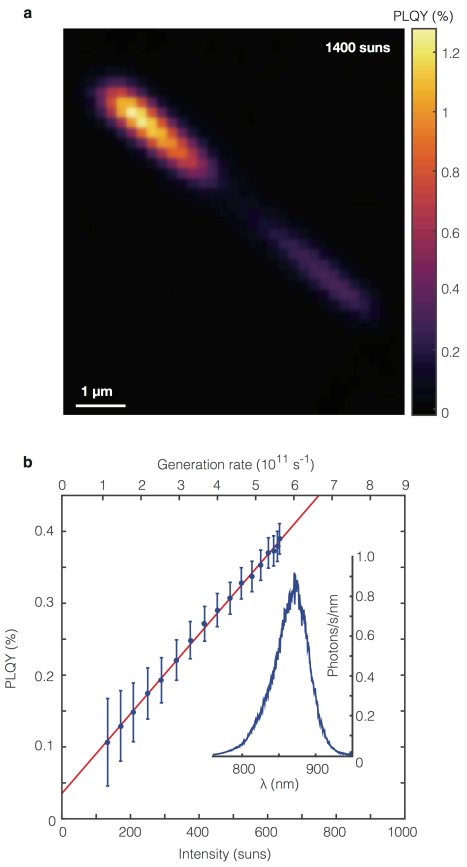

Figure 3 | Photoluminescence quantum yield and power dependence. The photoluminescence quantum yield, which is directly related to the V_{oc} of the device, is also determined using integrating sphere microscopy. **a.** A colour map of the photoluminescence quantum yield (PLQY) as a function of position, indicating that it peaks where the IQE is also highest (measured at 1400 suns to increase the signal to noise ratio). The scale bar is 1 µm. **b**. To determine the PLQY at 1 sun intensity we measured it for a range of intensities lower than in panel **a**. The experimental PLQY (blue dots) clearly shows linear behavior with intensity (supported by a linear fit in red), which indicates that Shockley-Read-Hall recombination dominates. The inset shows the nanowire photoluminescence (PL) spectrum at the brightest position in panel A, also at 1400 suns. All PLQY measurements were performed with 600 nm excitation light parallel to the nanowire axis. The measurement uncertainty is largely due to photodetector noise (see Methods).

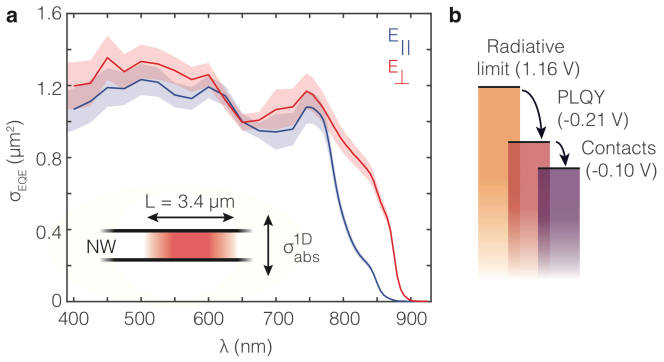

Figure 4 | Measuring thermodynamic limits and quantifying loss mechanisms in single nanowire solar cells. To determine the thermodynamic limit to the V_{oc} in a nanoscale solar cell we introduce the collection cross section σ_{EQE}, the nanophotonic equivalent of the external quantum efficiency (EQE). **a**. The collection cross section σ_{EQE} for polarisations perpendicular (red) and parallel (blue) to the nanowire axis as a function of wavelength. The collection cross section is the nanophotonic equivalent to the standard EQE for a macroscopic solar cell, but takes into account the effective area over which photons are absorbed. As shown schematically in the inset, this area is determined by multiplying the absorption width σ_{abs}^{1D} (see Methods) by the internal quantum efficiency (IQE) integrated over the nanowire length (see Fig. 2d). The shading displays the uncertainty, which is largely due to determination of the focused beam waist (see Methods). **b**. Based on σ_{EQE} we estimate the different contributions to the open-circuit voltage. The thermodynamic limit is V_{oc}^{rad} = 1.16 V, which is reduced by 210 mV due to the PLQY (non-radiative recombination in the semiconductor) to $V_{oc}^{imp} = 950\ mV$, and further reduced by 100 mV due to losses at the contacts, to a final V_{oc} of 850 mV.

Methods

Sample fabrication Nanowires are grown in a low-pressure Aixtron 200/4 Metal-Organic Vapor Phase Epitaxy (MOVPE) reactor, with the Selective Area MOVPE growth method. A 50 nm thick silicon nitride layer is used as Selective Area growth mask, patterned by the Soft Contact Nanoimprint Lithography technique[31,32] on a (111)A oriented p-doped InP substrate (Zn doping carrier concentration 2 x 10^{18} cm^{-3} from AXT, USA). Hydrogen (H_2) is used as a carrier gas for precursors, with a total flow of 15 l/min. Growth is performed at 730 °C with a pressure of 100 mbar, using tri-methyl-indium (TMI) and phosphine (PH_3) as precursors with molar fractions X_i (TMI) = 4.7 x 10^{-5} and X_i (PH_3) = 3.9 x 10^{-3}, resulting in a V/III ratio of 83. The total growth time is 11 minutes with a doping profile p^{++} / p / i / n / n^{--}, with respective segment growth times of 0.5 min / 3 min / 4 min / 3 min / 0.5 min (1 µm / 3 µm / 4 µm / 3 µm / 1 µm). We use diethyl-zinc (DEZn) as p-dopant, with molar fractions 1.3 x 10^{-5} in the p^{++} region and 6.4 x 10^{-6} in the p region. Di-tert-butylsilane (DTBSi) is used as n-dopant, with molar fractions 9.5 x 10^{-6} and 4.9 x 10^{-7} for n^{--} and n regions, respectively. After the growth, the wires were coated with a conformal 50 nm thick SiO_2 shell by plasma enhanced chemical vapor deposition, performed with silane and nitrous oxide as precursors at 300 °C. The nanowire measured in this paper had a total diameter of 410 nm (310 nm diameter InP), a length of 12 µm (9.8 µm between the contacts) and SiO_2 shell thickness of 50 nm. Supplementary Section 8 shows TEM images of wires grown with this method, highlighting the wurtzite crystal structure.

Au electrode patterns (see Supplementary Section 7) with alignment markers are fabricated on plasma cleaned glass substrates by UV lithography and metal evaporation. The nanowires are transferred from the arrays (~200 x 200 μm^2) via a pipette in ethanol and are randomly drop casted on the substrates. Electron beam lithography and metal evaporation are used to contact the single nanowires to the Au electrodes (see details below and Supplementary Section 7). It was found that the exact placement of the contact position on the highly doped end-segments of the nanowires is a crucial step to allow good ohmic contact and prevent extraction barriers. Then, the glass substrates are wire-bonded to glass holders, which have prefabricated metal contact lines (also by UV lithography and metal evaporation). The bottom of the glass holder is connected to a printed-circuit-board socket which also connects to a flat electrical cable extending outside of the integrating sphere (see Fig. 1c).

The metals used to contact the single nanowires were Ti (200 nm) and Au (30 nm) for the electron contact (on the n^{--} doped part) and Cr (~3 nm), Zn (15 nm), Au (215 nm) for the hole contact (on the p^{++}-doped part). Before the metal was evaporated, the exposed and developed substrates were etched in buffered HF (1:7, HF (49%): NH_4F (40%)) for 10 s to remove the protective SiO_2 shell (~50 nm) and the native oxide of the InP under the contact. The latter is known to cause Fermi-level pinning under the conduction band, which easily creates extraction barriers for the hole-contact[27]. The etched samples were transferred right away into the evaporation chamber to minimise the regrowth of the native oxide as much as possible. It is common to use an additional annealing step at high temperatures to

diffuse Zn into the p-type InP nanowire and create a highly p-doped layer[11]. We found this treatment to be damaging to our nanowires (strong decrease in photoluminescence efficiency) and therefore omitted this step, as the *in situ* doping of our nanowires allowed the formation of ohmic contacts even without annealing. Nevertheless, we chose to evaporate Zn for the hole-contact to prevent diffusion of Zn from the nanowire into the contact metal at elevated temperatures during the evaporation and lift-off steps.

For the electron contact, Ti and Au were evaporated with an electron beam evaporator at a pressure of ~5-10 x 10^{-7} mbar at an evaporation rate of 0.3-2 Å/s and acceleration voltage of 10 keV. For the hole contact Cr, Zn and Au were evaporated with a thermal evaporator at ~2x10^{-6} mbar at a rate of 0.2-1.5 Å/s.

Solar simulator measurement The I-V trace of the nanowire device is measured with a solar simulator (Oriel SOL2 94062A (6X6) Class ABA, Newport) with the AM1.5G spectrum at 1 sun (100 mW/cm^2) illumination intensity and an operating temperature of at most 50 °C, based on the temperature of a silicon reference cell. The lamp intensity of the solar simulator is adjusted with the same silicon reference cell. Electrical probes are used to contact the contact pads on the glass substrate with a source-measure unit (Agilent B2910). The voltage is scanned with a positive and negative scan rate between -1V and 1V in 2001 steps while the current is recorded (60 ms aperture and 70 ms delay between measurements). We observed no hysteresis in any of our measurements. Statistics on the performance of nanowire devices are discussed in Supplementary Section 9.

Electron beam-induced current measurement The electron beam-induced current (EBIC) measurements are conducted with a beam current of 100 pA and 5 kV acceleration voltage. The integration time per pixel is 10 μs. The position of the electron beam is synchronised with the read-out of the current signal which allows the superposition of the extracted current signal with the SEM image. From the profile of the EBIC intensity along the length of the nanowire we extract an electron diffusion length of $L_D = 285 \pm 10\,nm$ in the p-doped part of the wire (see Supplementary Section 1).

Integrating sphere microscopy The general measurement procedure for an absorption measurement is to prepare a sample on a glass substrate (it is crucial that the substrate is non-absorbing). The integrating sphere is positioned on a stage allowing it to be moved up and lowered to accommodate sample loading. The sample itself is positioned on a piezoelectric stage (required for scanning, to obtain local information) directly underneath the integrating sphere, which in turn is positioned on a mechanical stage. The sample is inserted into the integrating sphere through a narrow slit in the bottom of the sphere, to minimise exposed open aperture area in the integrating sphere. The integrating sphere photodetector is positioned behind a baffle to prevent direct illumination of the detector, as can be seen in Fig. 1c.

The absorptance of a sample in an integrating sphere is typically given by $A = 1 - IS_s/IS_r$, where IS_s is the integrating sphere photodetector signal when

illuminating the sample and IS_r when the incident beam misses the sample (the reference)[22]. Normally the sample inside the integrating sphere is slightly tilted, such that the specular reflection stays inside the integrating sphere. Here, however, tilting the sample is impractical due to the use of an objective. Hence, we have to add an additional photodetector to detect reflected light (see Fig. S3), and an additional term to the standard equation to account for reflected light:

$$A = 1 - \frac{R_S}{R_r} - \frac{IS_S}{IS_r} - 0.04 \qquad \text{(Eq. 2)}$$

where A is the absorptance, R_s and R_r are the reflection and reflection reference measurements to account for detection sensitivity. The additional 0.04 is a correction factor to account for the reflection from the second interface of the glass slide, which goes back into the objective but is not collimated (as it is far out of focus) and therefore not detected. As a result 4% is missing from the power balance, which is accounted for in Eq. 2. We have implicitly assumed here that this reflection loss is constant, but in reality it slightly decreases or increases with the amount of forward scattered and transmitted light. Hence, it is a small source of error: for example, if 20% of the incident beam is absorbed by a non-scattering particle, this will lead to a reduction of this reflection loss to 3.2%. Thus, by subtracting a constant offset, a small error in the absorptance is introduced. The reference measurements in Eq. 2 are done by placing a mirror (Thorlabs PF10-03-P01) in the focal plane of the objective for the reflection reference, while for the integrating

sphere reference measurement the focused beam is achieved by focusing the light through a hole drilled in the sample (a “miss”).

In this experiment we use a supercontinuum laser (Fianium WL-SC-390-3), sent through an acousto-optical tunable filter (AOTF, Crystal Technologies, ~5 nm bandwidth). The long working distance objective required for illuminating the samples is a Mitutoyo M Apo Plan NIR 50x NA 0.42 objective with a 17 mm working distance. The integrating sphere is a custom modification to a GPS-020-SL integrating sphere built by LabSphere, modified to accommodate the objective lens. We use low-noise Newport 818-UV calibrated photodiodes, each connected to Stanford Research Systems SR830 lock-in amplifiers. The transmission of the acousto-optic tunable filter was digitally modulated with a 50 percent duty cycle as a source for the lock-in amplifiers. The sample was mounted on a 3D piezoelectric stage (Piezojena Tritor400), which itself was mounted on a Newport mechanical stage for rough alignment. The incident intensity was controlled with ND filters (Thorlabs) and the AOTF RF power. The incident light is ensured to be linearly polarised by sending it through a polarising beam splitter, and the polarisation is then rotated to the desired orientation using a half-wave plate (both Thorlabs). The orientation of the nanowire was determined from an absorption map. See Supplementary Figure 3 for a full schematic diagram of the experimental set-up and additional information.

To verify that with integrating sphere microscopy we can indeed measure absorptance accurately, we measured the "absorptance" on silica (SiO_2) nanobeads. While they do not absorb, they scatter strongly, providing us with a means to

determine the collection efficiency of scattered light. Based on the ratio of detection loss in the integrating sphere to total extinction for the nanosphere we estimate that 95±1.2% of the scattered power is collected (see Supplementary Section 4).

For measurements on the nanowire solar cell we use very low powers (< 1 nW) to achieve intensities close to 1 sun. We therefore used Newport 818 series photodetectors, which have a low noise-equivalent power, connected to SR830 lock-in amplifiers. The nanowire solar cell is connected to an SR830 lock-in amplifier as well, and incident power is modulated with 195 Hz, below the cut-off frequency of the nanowire device. Calibration of the incident power is done by placing one of the calibrated Newport 818-UV photodiodes directly in front of the objective.

Photoluminescence measurements An integrating sphere is also commonly used to measure photoluminescence quantum yield (PLQY) quantitatively, either by connecting a spectrometer to the integrating sphere or by using a combination of long- and shortpass filters[22]. To measure the PLQY on the nanowire we use a longpass filter in front of the integrating sphere detector (Thorlabs FELH0750). The PLQY at low intensities is not high enough to require a shortpass filter for accurate absorption measurement. The photoluminescence collection efficiency of the integrating sphere is determined by sending monochromatic light over the wavelength range of photoluminescence into the integrating sphere, but missing the sample. The total photoluminescence detection efficiency η_{PL} (Coulombs/emitted photon) can then be calculated using:

$$\eta_{PL} = \frac{\int S(\lambda)\eta(\lambda)d\lambda}{\int S(\lambda)d\lambda} \quad \text{(Eq. 3)}$$

Here $S(\lambda)$ is the PL spectrum (shown in the inset in Fig. 3b), and η is the wavelength dependent collection efficiency of the integrating sphere (also in Coulombs/photon). The PLQY is then calculated as the number of emitted photons divided by the number of absorbed photons.

Measurement uncertainty Figs. 2e, 3b, and 4a show shaded areas corresponding to the measurement uncertainty in each of these measurements. These areas indicate the standard deviation, which were determined following regular error propagation rules for each of the individual signals. For example, the IQE (shown in Fig. 2e) is given by $IQE = \hbar\omega I/(qP_{abs})$, where $\hbar\omega$ is the photon energy, I is the photocurrent, q is the electron charge, and P_{abs} is the absorbed power. Denoting the standard deviation by δ, we find for the measurement uncertainty:

$$\delta IQE = IQE\sqrt{\left(\frac{\delta I}{I}\right)^2 + \left(\frac{\delta P_{abs}}{P_{abs}}\right)^2} \quad \text{(Eq. 4)}$$

The absorbed power itself is determined through Eq. 2, for which a similar procedure is followed. Due to the low incident power the photodetector noise contained in P_{abs} dominates for Figs. 2e and 3b, while for the cross sections in Fig. 4a fitting of the spot size dominates the measurement uncertainty, which can be further improved.

Determining the collection cross section The total current generated under given illumination intensity at wavelength λ is given by:

$$I(\lambda) = q \int IQE(\boldsymbol{r}) \frac{P_{abs}(\boldsymbol{r})}{hc/\lambda} \, dV \,, \qquad \text{(Eq. 5)}$$

Here q is the electron charge, $IQE(\boldsymbol{r})$ is the local collection efficiency, $P_{abs}(\boldsymbol{r})$ is the locally absorbed power, and the integral is over the volume of the nanostructure. To obtain a quantity that is normalised to the incident intensity (i.e. equivalent to the external quantum efficiency), we express Eq. 5 in terms of absorption cross sections. For a horizontal single nanowire the absorption cross section (which is an area, 2D) is typically expressed in absorption cross section per unit length of the nanowire, such that an effective absorption width (1D) is obtained. The total absorption cross section is then effectively obtained by multiplying by the length of the wire. Since we are interested in the collection cross section, the relevant length of the wire is given by the active length shown in Fig. 2d, which thus leads to Eq. 1:

$$\sigma_{EQE}(\lambda, \Omega) = \int IQE(\lambda, z) \, \sigma_{abs}^{1D}(\lambda, \Omega) \, dz \,, \qquad \text{(Eq. 6)}$$

where σ_{abs}^{1D} is the absorption width of the nanowire (indicated by the superscript 1D). The effective absorption width σ_{abs}^{1D} can be retrieved from the absorptance measurement using a simple formula:

$$\sigma_{abs}^{1D}(\lambda) = A\, w_0 \sqrt{\pi/2}\,, \qquad \text{(Eq. 7)}$$

Here A is the absorptance and w_0 is the beam waist (defined formally in the next paragraph). This formula can be found by considering the Gaussian intensity distribution of the focused spot:

$$I(x,z) = I_G\, e^{-2\left(\frac{x^2}{w_0^2}+\frac{z^2}{w_0^2}\right)} = \frac{2P_{in}}{w_0^2} e^{-2\left(\frac{x^2}{w_0^2}+\frac{z^2}{w_0^2}\right)} \qquad \text{(Eq. 8)}$$

where I_G is the Gaussian peak intensity (in W/m^2) and P_{in} is the total power carried by the beam (in W). The beam waist w_0 is defined as the radius at which the intensity is I_G/e^2. When the wire is subject to inhomogeneous illumination, as with a Gaussian spot, the total absorbed power is found by integrating the intensity along the nanowire, where we assume that we can ignore the intensity gradient over the width of the nanowire (i.e. the wire is infinitely thin):

$$P_{abs} = \int \sigma_{abs}^{1D}\, I(x=0,z)dz \qquad \text{(Eq. 9)}$$

where for simplicity we assume that the wire is aligned along the z-axis. Combining with Eq. 8 and 9 we find Eq. 7, where $A = P_{abs}/P_{in}$. This formula has been applied before to carbon nanotubes[17]. Although the assumption is made that the wire is infinitely thin, agreement between this approximation and full-wave simulations is good (see Fig. S5). Experimentally we did not observe a dependence of the

absorption cross section on the spot size, which we checked by underfilling our objective until the spot size was increased by 60%. It is important to note that absorptance measurements with the focused spot are possible for all sizes, but that only conversion to an absorption cross section becomes complicated for large diameter nanowires when using a tightly focused spot. This problem can be mitigated, however, by using a larger spot size (thus at the cost of spatial resolution).

It is also important to note that σ_{EQE} can also be determined directly from the beam waist, the incident photon flux, and the laser induced photocurrent: $\sigma_{EQE}(\lambda) = w_0 \sqrt{\pi/2} \int (I_L(z)/S_{in})\, dz$, where I_L is the laser induced photocurrent, S_{in} is the total incident photon flux, and the integral again is over the nanowire length. With this approach σ_{EQE} can be determined with any laser-beam induced current (LBIC) set-up. Additionally, the experimental error will be smaller since both I_L and S_{in} can be determined accurately. For that reason we have determined σ_{EQE} in Fig. 4 following this approach.

References for the Methods section

31. Mårtensson, T. *et al.* Nanowire arrays defined by nanoimprint lithography. *Nano Lett.* **4,** 699–702 (2004).
32. Pierret, A. *et al.* Generic nano-imprint process for fabrication of nanowire arrays. *Nanotechnology* **21,** (2010).